Realising a biomimetic low-Vogel-exponent aquatic training device

Bioinspiration &
Biomimetics

NOTE • **OPEN ACCESS**

Realising a biomimetic low-Vogel-exponent aquatic training device

Bioinspiration & Biomimetics

NOTE

Realising a biomimetic low-Vogel-exponent aquatic training device

Derian D Espinosa[1,2], **Henry León-Ariza**[3,*] and **Arion Pons**[4,*]

[1] Doctoral Programme in Biosciences, Universidad de La Sabana, Chía, Colombia
[2] Faculty of Bioengineering, Universidad Santo Tomás, Bogotá, Colombia
[3] Faculty of Medicine, Universidad de La Sabana, Chía, Colombia
[4] Department of Mechanical Engineering, Chalmers University of Technology, Gothenburg, Sweden
[*] Authors to whom any correspondence should be addressed.

E-mail: henry.leon@clinicaunisabana.edu.co and arion@chalmers.se

OPEN ACCESS

RECEIVED
24 February 2026

REVISED
6 May 2026

ACCEPTED FOR PUBLICATION
27 May 2026

PUBLISHED
22 June 2026

Keywords: Vogel exponent, aquatic training, resistance training, structural flexibility, swimming parachute

Supplementary material for this article is available online

Abstract

Aquatic resistance training is a key technique within both sports training and osteomuscular rehabilitation, typically featuring the use of devices such as swimming parachutes to augment the hydrodynamic drag of the trainee. Conventional swimming parachutes, however, are limited by the classical strong (quadratic) scaling of drag force with velocity: to maintain a consistent target resistance, the swimmer must maintain a constant speed and the parachute size must be closely adjusted to this speed. In this work, we present and evaluate a bio-inspired approach to overcome these limitations. Many flexible biological structures, both terrestrial and aquatic, show weakened drag-velocity scaling, and thereby more consistent drag loading: an effect measured by the Vogel exponent ($\mathcal{V}$). We design a swimming parachute with squid-inspired morphology that uses structural flexibility to weaken drag-velocity scaling, and evaluate it experimentally under the hydrodynamic conditions associated with crawl swimming. This evaluation confirms low Vogel exponent ($-0.9 < \mathcal{V} < -1.3$), corresponding to linear-to-sublinear scaling of drag force with velocity, across several different morphological configurations. This demonstration of improved resistance load consistency via flexible bio-inspired morphology has the potential to reduce the risk of injury in aquatic resistance training, and provides a novel connection between biological fluid-structure interaction and biomedicine.

Nomenclature:

Drag force	F_D, N
Velocity	U, km h^{-1} and m s^{-1}
Vogel exponent	$\mathcal{V}$
Reynolds number	Re
Disk nominal radius	r, cm
Confidence interval	CI
Elastic modulus	E, GPa
Density	ρ, kg m^{-3}

1. Introduction

Effective physical training in sports and rehabilitation often requires increasing movement resistance. The purpose of increasing resistance during training is to elevate muscular tension, thereby placing stress on the musculoskeletal tissue [1]. This stress increases oxygen consumption and energy production, promoting long-term adaptations such as improvements in muscular strength, tone, and trophism [2]. Resistance aquatic training has been shown to be beneficial for swimmers' performance [3] as well as for patients with various musculoskeletal conditions [4].

A wide range of devices—including swimming parachutes, drag suits, hand paddles, fins, and specialised boots and barbells [5]—are available for generating aquatic resistance, which is produced by hydrodynamic drag (F_D) resulting from the interaction between the water and the moving device [6]. At flow regimes associated with human swimming, the magnitude of this force typically depends on the square of its velocity (U, $F_D \propto U^2$), assuming that the device is a rigid body [7, 8]. This strong velocity dependence makes it difficult to maintain a

constant target resistance load [1, 9], forcing trainers and rehabilitators to try to approximate target loads via device size and movement cadence [1, 10–12]. This contrasts with resistance control in training and therapy on dry land, where training-load can be precisely regulated through quantifying the weight moved [13, 14]. Improvements to load control within aquatic resistance training would offer several benefits: well-managed training-loads reduce the risk of injury and enables training plans with gradual resistance progression [15]. This in turn facilitates nervous system adaptation, including improvements in cortical representation [16] and motor rehabilitation [16, 17].

The question of the strength (or, weakness) of drag scaling with velocity has seen significant study in another field: biological and bio-inspired fluid-structure interaction. It is well known that a wide range of flexible structures [18], including in plant [8, 19, 20] and animal [8, 21, 22] morphology, show drag scaling lower than quadratic. In this context, Vogel [23] defined what has come to be termed the *Vogel exponent* ($\mathcal{V}$):

$$F_{\mathrm{D}} \propto U^{2+\mathcal{V}}. \tag{1}$$

In botany, several previous studies have quantified $\mathcal{V}$ for different plant species—leaves, branches, or whole specimens—in both aquatic and terrestrial environments [19, 20], with exponent values ranging from 0 to −1.3. This weakened drag scaling increases the survivability of vegetation against wind [24] and water [19] loading. In engineering fluid-structure interaction, previous studies have focused on the characteristics of ideal rectangular plates ($\mathcal{V} = -1.4$), cut disks ($\mathcal{V} = -1.1$) [18], beams ($\mathcal{V} \approx -0.86$) [25] and bluff bodies with rear flexible plates ($\mathcal{V} \approx -0.1$). The latter have been suggested for drag reduction applications in heavy transport [26]. A range of computational [27] and reduced-order models [28, 29] for different ideal configurations have been developed. However, to the authors' knowledge, no Vogel-type studies have previously been conducted for rehabilitation and sports training applications, nor have any applications of the Vogel exponent in other fields, such as transport, reached the level of validated physical prototypes.

This study introduces one such application and prototype: a potential solution to the challenge of strong drag-velocity scaling (i.e. load inconsistency) of conventional swimming parachutes [6, 9], via bio-inspired flexible morphology. We propose and design a swimming parachute [6] with a flexible folded cut-disk morphology, inspired by squid arms—squid operate at Reynolds numbers similar to those of human swimming [30, 31]. In addition, to explore the dependency of scaling on morphology and provide further avenues for resistance load management, the parachute cut-disk morphology is evaluation of the drag-velocity scaling of this novel parachute, under conditions that are representative of human crawl swimming, and identify power-law and polynomial models describing the relationship between F_{D}, U, and adjustable radius (r). This evaluation confirms significantly weakened drag-velocity scaling, with Vogel exponents showing a trend from −0.9 (mildly superlinear scaling) at minimum radius, to −1.3 (sublinear scaling) at maximum radius. In comparison to existing swimming parachutes [6, 9], drag loads are significantly more consistent with velocity: a potential solution to the challenge of consistent loading in aquatic resistance training [1, 9]; and a novel connection between bio-inspired fluid-structure interaction and biomedicine.

2. Methods

2.1. Bio-inspired training device design

Figure 1 illustrates the design and intended use of a squid-inspired aquatic training device, analogous to a swimming parachute [6, 9]. The principle of the design is as follows. A swimmer wears a belt with a rope attached to the device, which comprises a cut and folded disk connected to a hollow shell within which is a buoyancy chamber. The cut disk is constructed from polyethylene terephthalate (PET, $E = 3.7$ GPa, $\rho = 1.33$ kg m^{-1} [32]) sheet of thickness 0.3 mm. PET is chosen for accessibility and consistency with prior Vogel exponent studies [33, 34], though we note that it differs from the textiles used in swimming parachutes [6, 9]. The cut disks of the device can be retracted into the hollow shell, enabling adjustment of the nominal radius of the disk (r) to seven levels, corresponding to different levels of overall load: this adjustability allows us to study the effect of device r on drag-velocity scaling, and would enable trainers or rehabilitators to adjust the target resistance prior an aquatic training session [5] The design draws inspiration from the flexibility of squid arms [35, 36] and their (actuated) flexion during hunting activities [37]. Moreover, Reynolds numbers in squid swimming (Re $\approx 10^3$ -10^6 [30]) are comparable to those in human swimming ($Re \approx 6.6 \cdot 10^5$-$3.9 \cdot 10^6$ [31]).

2.2. Experimental design

Consistent with previous studies [6], the device was submerged at neutral buoyancy just below the surface of an artificial lake (1.5 m deep, freshwater at 13°C) within the campus of Universidad Militar Nueva Granada in Colombia. It was towed via a non-elastic rope by an electric scooter (*Xiaomi 3*) over a distance of 10 m, measured by ground marks, and starting from rest (figure 2(a)). This distance is commensurate with that required for a human swimming crawl to reach target speeds [38]. Considering the tension force in the rope during steady motion to represent hydrodynamic drag, as in previous studies [6], a Pasco

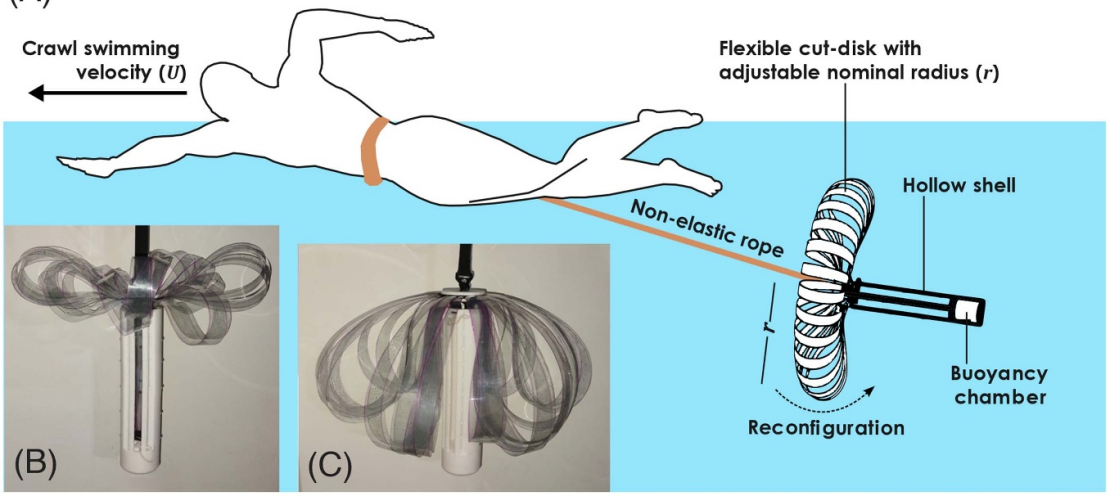

Figure 1. A bio-inspired flexible swimming parachute for aquatic resistance training (a) Schematic of the squid-inspired parachute, and illustration of its use in aquatic resistance training. (b) and (c) Photograph of a prototype device, illustrating flexion of the cut-disk morphology—here, under gravity, as an illustrative simulation of hydrodynamic drag.

PS-2104 force sensor (figure 2(a)) was used to measure tension [39] with a sampling frequency of 1 *kHz*. To coordinate distance and time, force sampling was started and stopped manually before and after the towing period—though we note that the rope generally started slack, and that the manual sampling stop was slightly delayed with respect to the 10 m mark. We account for this both effects when processing data (Section 2.3). During the last meters on the marked trail, the scooter speed was monitored on its control panel, aiming to maintain a speed variation below 10%, commensurate with the intracycle velocity variation in crawl swimmers [6].

Experiments were conducted in triplicate, across velocities in the range reported by Fernandez *et al* [39] for crawl swimming (2-7 km h^{-1})—the most common swimming style—, and across seven different load levels, corresponding to the following adjustable radii (r): 52, 55, 58, 61, 64, 67, and 70 cm, commensurate with the dimensions of commercial swimming parachutes [5]. Our design of experiment is to first capture a complete univariate dataset for each of parameter in isolation: velocity, at nominal radius $r = 70$ cm; and radius, at velocity of 4 km h^{-1}—this latter velocity was chosen as the average speed of professional crawl swimmers with resistance [40]). We then capture a limited range of additional datapoints to capture the multivariate relationship between drag, velocity, and radius: specifically, for $r = 64$ and 67 cm, velocities 2, 4 and 5 km h^{-1}, and for the remaining radii ($r = 52$; 55; 58; and 61 cm), velocities 2 and 4 km h^{-1}. The full dataset of force measurements can be found in the supplementary material.

2.3. Data processing

Force time signals were processed as follows. (**i**) Signals were subjected to low-pass filtering to remove noise. (**ii**) Signals were clipped in time to before the sudden force drop due to deceleration after the 10 m mark—providing an approximate time-distance synchronisation. (**iii**) Only the last 20% of the remaining signal was extracted as the drag force (F_D)—to ensure that the test speed had been reached, the rope was in tension, and the disk flexion had reached steady state. To illustrate this processing, figure 2(b) presents a force signal vs time (s) and distance (m) for $r =$ 70 cm at 7 km h^{-1}, To determine $\mathcal{V}$, we apply power-law regression over mean F_D and U, following the botanical studies of Bekkers *et al* [24] and Zhang *et al* [41]. We then perform linear regression over $\mathcal{V}$ and r; and polynomial regression over F_D and r. Finally, we perform multivariate regression over F_D, r and U, informed by univariate models.

3. Results

3.1. Weakened scaling of drag force with velocity

To characterise the relationship between hydrodynamic drag (F_D) and swimming velocity (U), and thereby determine the Vogel exponent ($\mathcal{V}$), we performed a power-law regression [24, 41], of the model:

$$F_D = aU^b \tag{2}$$

where $\mathcal{V} = b - 2$. Box-and-whisker plots of experimental measurements of F_D for each U for a load level with $r = 70$ cm are presented in figure 3, the power-law regression of equation (2), with $a = 14.33$ and $b = 0.71$ ($\mathcal{V} = -1.29$), alongside drag measurements reported for a 1600 cm^2 commercial swimming parachute [9]. The regression characterises the data well ($R^2 = 0.97$). Compared to the conventional swimming parachute [6, 9], the bio-inspired device

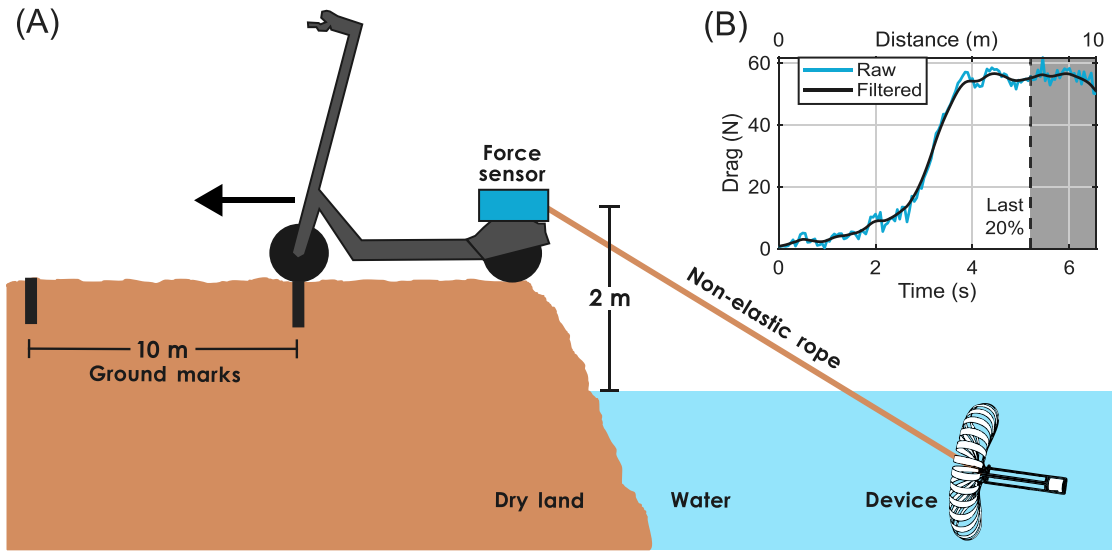

Figure 2. (a) Illustration of experimental setup. (b) Example of drag measurement vs time and distance for load level (nominal radius) of 70 cm at 7 km h^{-1}.

shows significant weakening in the scaling of drag force with velocity: sublinear, rather than quadratic, scaling is observed, with $\mathcal{V} = -1.29$. This value is consistent with theoretical estimates of the Vogel exponent of a flexible cut disk rolling into a cone, as per Gosselin *et al* [18] ($\mathcal{V} = -1.33$). These results suggest that bio-inspired flexion is a pathway to maintaining aquatic training loads that are as constant as possible with swimming speed.

3.2. Dependency of Vogel exponent on nominal (adjustable) radius

Figure 4 shows Vogel exponent ($\mathcal{V}$) estimates obtained via power-law regression (Section 3.1) for each load level setting (adjustable nominal radius, r). Vogel exponent estimates range from -0.99 to -1.29: consistent linear to sublinear scaling of drag force with velocity at all load level settings, in contrast to the traditional swimming parachutes described by Cortesi *et al* [6] and Coloretti *et al* [9]. These values are lower than those reported for plants [19, 20], but higher than those reported for flexible plates ($\mathcal{V} = -1.4$) [18]—the latter, likely due to the flow between the disk's cuts, as per Gosselin *et al* [18]. The full dataset of power-law regressions can be found in the supplementary material.

We observe a trend of decreasing Vogel exponent (i.e. further weakening of drag-velocity scaling) with nominal radius. We characterise this trend with a linear regression:

$$V = cr + d, \tag{3}$$

and identify $c = -0.01$ and $d = -0.24$, with high coefficient of determination ($R^2 = 0.81$). Physically, larger r increases the cut disk's flexibility, as well as the drag contribution of the cut disk relative to that of the bluff-body hollow shell. In the idealised framework of Leclercq & de Langre [28], these might be considered to be a combination of both material (ψ) and geometrical (ϕ) parameters, though distinguishing which is more significant in the context of this device is challenging. We note also that this linear regression will not hold asymptotically: at sufficiently high U and r—i.e. large Cauchy number [28]—flexion will completely align the disk with the flow and $\mathcal{V}$ will converge.

To confirm that this trend is not a result of the changing window of velocity over which the power-law regression is performed, we perform an additional two-point Vogel exponent estimate using data for 2 km h^{-1} and 4 km h^{-1}, which was captured for all nominal radii. For any pair of force–velocity datapoints ($F_{D,1}$, U_1 and $F_{D,2}$, U_2), the Vogel exponent is exactly determined by:

$$V = \frac{\ln(F_{D,1}/F_{D,2})}{\ln(U_1/U_2)} - 2. \tag{4}$$

Figure 4 illustrates these further estimates, which confirm the trend of decreasing Vogel exponent with nominal radius.

3.3. Sub-quadratic scaling of drag force with nominal radius

Figure 5 illustrates the relationship between drag force and nominal radius for the representative case of 2 km h^{-1} velocity. In the case of a rigid disk undergoing isometric scaling, the relationship between drag force and radius would be roughly quadratic, based on the scaling of frontal area [7, 8]. However, the flexible device shows notably weaker scaling. We quantify this with a second-order polynomial regression of the form:

$$F_D = er^2 + fr \tag{5}$$

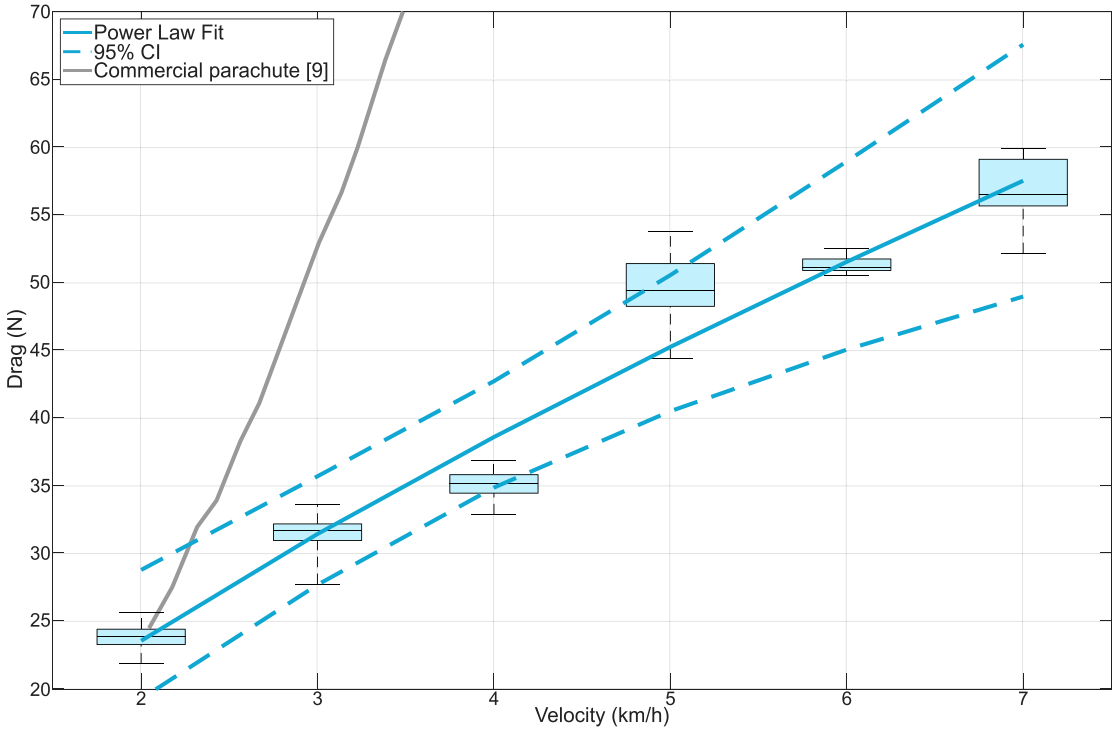

Figure 3. Box-and-whisker plots of drag force scaling with velocity, alongside the power-law regression, for device nominal radius of 70 cm. For comparison, reported drag force results for a conventional 1600 cm^2 swimming parachute [9] are overlaid. Across velocities commensurate with crawl swimming, significant weakening of the drag force scaling is observed, down to sublinear levels ($\mathcal{V} = -1.29$).

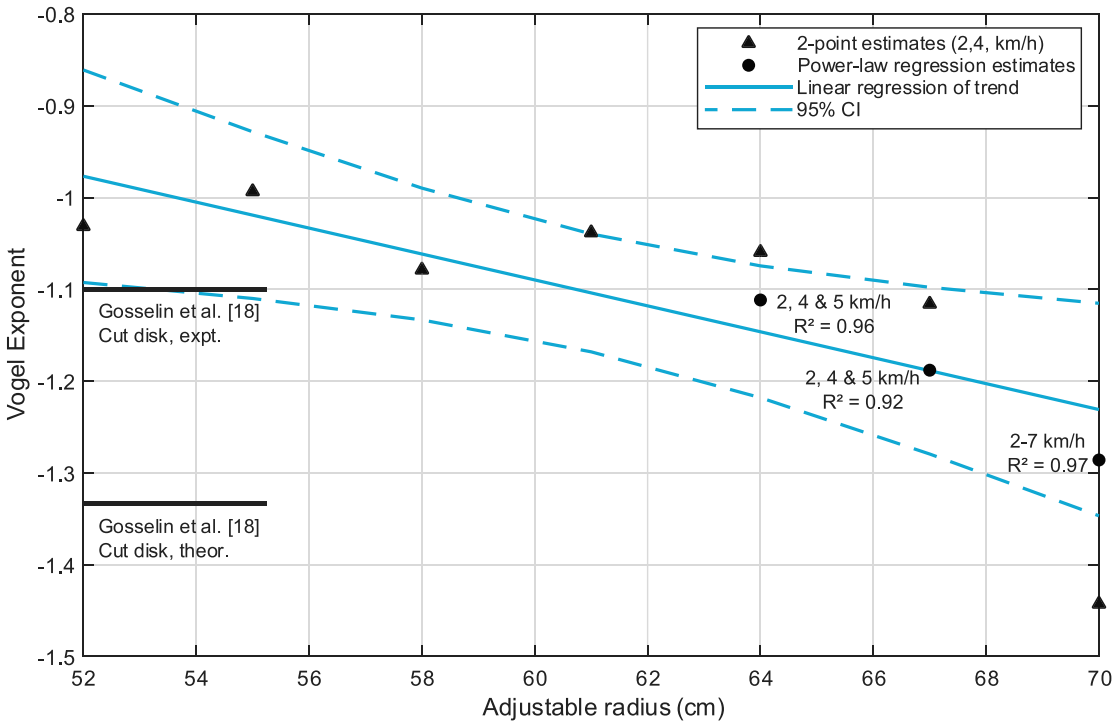

Figure 4. Computed Vogel exponents ($\mathcal{V}$) for each nominal radius, both for the full power-law regression and the two-point estimate: a trend of decreasing $\mathcal{V}$ with r is observed. Velocity windows, and the power law coefficient of determination, are indicated, alongside comparable Vogel exponent values from the literature.

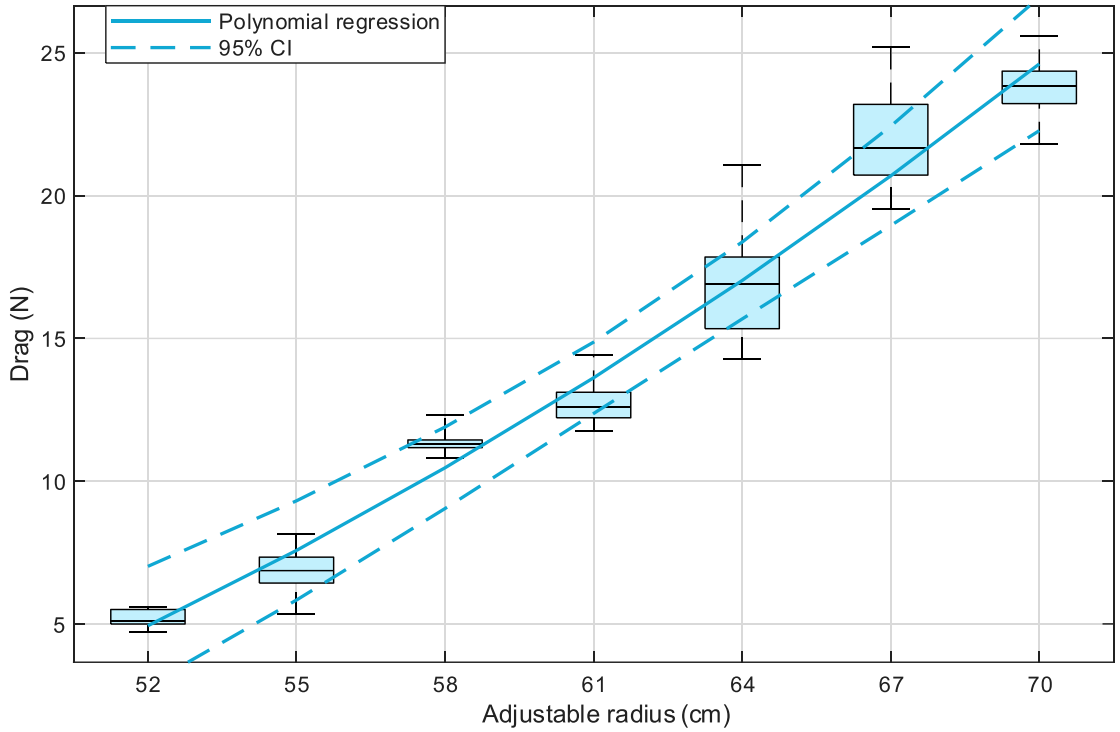

Figure 5. Box-and-whisker plots of drag forces against nominal radius (i.e. load level setting), for the representative case of 2 km h^{-1} velocity. Near-linear scaling is observed,

where the coefficient f accounts for weakened scaling. Regression results for 2 km h^{-1} ($e = 0.01$ and $f = -0.65$, figure 5) and 4 km h^{-1} ($e = 0.02$ and $f = -0.64$) indicate scaling that is nearly linear (rather than quadratic). Several factors may account for this weakened scaling, including (**i**) the trend in Vogel exponent with radius (figure 4), leading to more extreme flexion at larger radii; (**ii**) the non-isometric scaling associated with increasing the cut-disk radius, leading to a reduction in effective frontal area at larger radii—analogous to effects observed by Gosselin *et al* in flexible plate tests at higher speeds [18]; and (**iii**) a transition in dominance from form drag to skin friction drag as the nominal radius and degree of flexion increases, leading ultimately (for large radius) a seaweed-like pattern of reconfiguration [19, 20].

3.4. Multivariate relationships

The univariate relationships identified in Section 3.1–3.3 can themselves be assembled into an approximate multivariate relationship between drag, velocity and nominal radius—as illustrated in figure 6. The question then arises of what multivariate model is appropriate for this relationship. We consider first the combination of a velocity power law (U^b) and quadratic radius scaling (r^2):

$$F_D = ar^2U^b \tag{6}$$

corresponding to the assumption of a Vogel exponent that remains completely constant. Figure 6 illustrates regression of this model to the experimental data. Despite capturing the overall trend ($R^2 = 0.91$), there are observable discrepancies, particularly in the scaling of drag with radius. We then consider a possible extension to this model, based on the linear dependency of Vogel exponent on radius identified in Section 2.2:

$$F_D = ar^2U^{cr+d}. \tag{7}$$

This extension leads only to a marginal improvement in goodness of fit ($R^2 = 0.94$) and does not resolve the discrepancies in the scaling of drag with radius. In addition, regression of equation (7) identifies an increasing trend of Vogel exponent on radius ($c > 0$), inconsistent with univariate results (figure 4). From this we conclude that the sub-quadratic scaling of drag with radius—identified in Section 3.1–3.3, and reflected in the multivariate relationship—does *not* stem primarily from a dependency of Vogel exponent on radius, but must arise from other factors, such as the non-isometric scaling of the device and the balance of form and skin friction drag. Extensions to existing reduced order-models of flexible reconfiguration, e.g. [28, 29], might offer more effective multivariate models for this device.

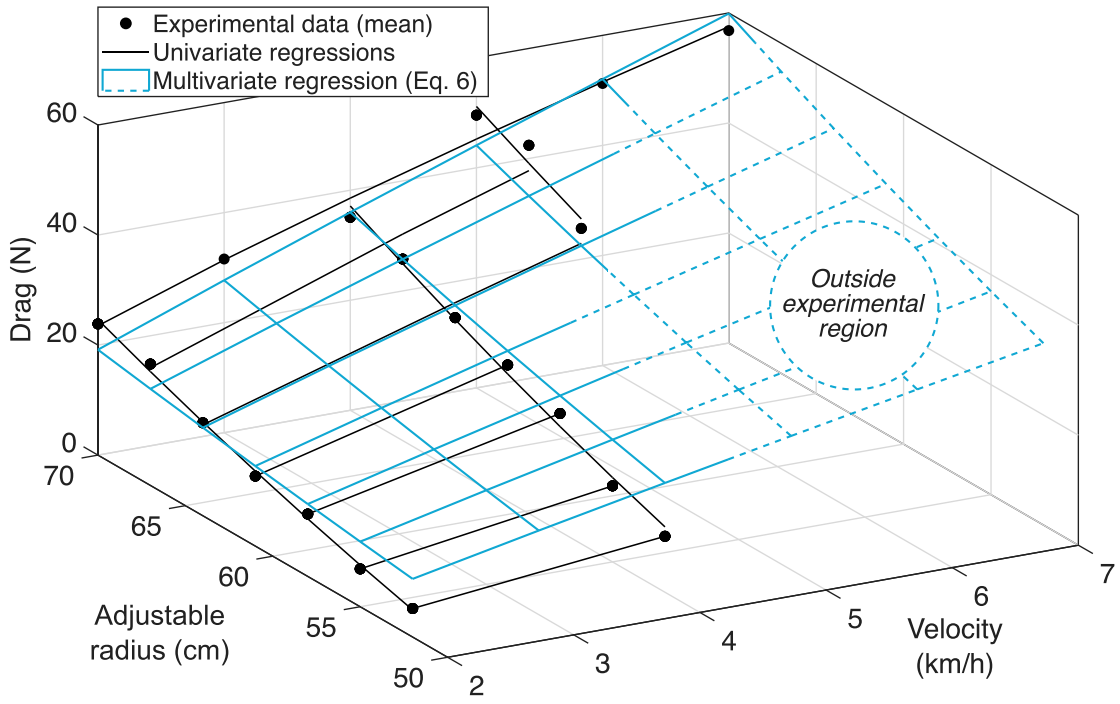

Figure 6. Surface of multivariable model of the relationship between drag forces, adjustable nominal radius (i.e. load level setting), and velocity. Full data sets, and mean drag, are indicated, alongside polynomial and power-law regressions.

4. Discussion and conclusion

This work establishes a novel connection between biological flow control and biomedicine. It proposes a biomimetic device as a potential solution to aquatic training-load management challenges by weakening the scaling of hydrodynamic drag force with velocity. Inspired by squid morphology, the biomimetic device functions like a swimming parachute, but features a flexible cut-disk geometry with adjustable load levels. Tested under realistic crawl swimming conditions, we identify power-law and polynomial models for this device that describe the relationships between hydrodynamic drag (F_D), swimming velocity (U), and loads level (adjustable nominal radius, r). We demonstrate: (**i**) consistently low Vogel exponents across all load level settings, corresponding to sublinear drag-velocity scaling—substantially weaker than traditional swimming parachutes [6, 9]; (**ii**) a trend of decreasing Vogel exponent with nominal radius, indicating the presence of complex fluid and structural scaling effects; and (**iii**) a multivariable model relating F_D, U and r for practitioners. This device represents the first application of the Vogel exponent in rehabilitation and sports training, as well as a novel step in Vogel exponent studies from theory into the field: a validated prototype of a Vogel-type device. Future evaluation should examine how the device responds under human swimming wakes, as prior studies have reported a 15 % reduction of conventional parachute resistance when towed by a propelling swimmer [9]. Such evaluation should also assess the effect of transient velocity variations—such velocity variation is also known to have significant effects on conventional swimming parachutes [6]. Water tunnel experiments, rather than the simulated open-swimming experiments of this work, would be better suited to assessing these effects.

In summary, our results suggest that aquatic training devices that utilise bio-inspired structural flexion could address the challenge of maintaining near-constant training load in underwater resistance training [1, 9]. They provide renewed motivation for studies of the fundamental mechanics of structural flexibility in fluid flow, particularly for complex geometries such as the folded cut-disk used in this study, which has not previously received theoretical characterisation. They also motivate clinical study into whether reconfiguration-based sublinear drag-velocity scaling yields improvement in underwater training outcomes [9]. And finally, given the close relationship between bio-inspired and biological (particularly, botanical) flow-induced structural reconfiguration, the possibility of biohybrid devices for sports training and rehabilitation arises—perhaps plant morphology itself can provide an accessible and sustainable training tool?

Acknowledgements

D.D.E. was supported by the Universidad de La Sabana under the Convocatoria Interna para el Apoyo a Proyectos de Tesis Doctorales 2022-2–2024-1, 5th cort; foundations managed by The Royal Swedish Academy of Sciences; and by an award from the Chalmers Area of Advance Health Engineering (2025-0025-20) to A.P.

Data availability statement

Alldata that support the findings of this study are included within the article and (supplementary files). Supplementary Material available at https://doi.org/10.1088/1748-3190/ae73d5/data1.

Author contributions

Derian D Espinosa 0000-0003-1705-8922
Conceptualization (lead), Data curation (equal), Formal analysis (equal), Funding acquisition (equal), Investigation (lead), Methodology (equal), Resources (equal), Software (equal), Validation (lead), Visualization (lead), Writing – original draft (equal)

Henry León-Ariza 0000-0002-5557-2060
Conceptualization (supporting), Funding acquisition (equal), Methodology (supporting), Project administration (supporting), Supervision (equal), Writing – review & editing (supporting)

Arion Pons 0000-0001-6102-1735
Data curation (equal), Formal analysis (equal), Funding acquisition (equal), Project administration (lead), Resources (equal), Software (equal), Supervision (lead), Writing – original draft (equal), Writing – review & editing (lead)

References

[1] Colado J C and Triplett N T 2009 Monitoring the intensity of aquatic resistance exercises with devices that increase the drag force: an update *Strength Cond. J.* **31** 94–100
[2] De Souza A S, Pinto S S, Kanitz A C, Rodrigues B M, Alberton C L, Da Silva E M and Kruel L F M 2012 Physiological comparisons between aquatic resistance training protocols with and without equipment *J. Strength Cond. Res.* **26** 276–83
[3] Ramos Veliz R, Requena B, Suarez-arrones L, Newton R U and Sáez de Villarreal E 2014 Effects of 18 week in season heavy resistance and power training on throwing velocity, strength, jumping, and maximal sprint swim performance *J. Strength Cond. Res.* **28** 1007–14
[4] Frohman A N, Okuda D T, Beh S, Treadaway K, Mooi C, Davis S L, Shah A, Frohman T C and Frohman E M 2015 Aquatic training in MS: neurotherapeutic impact upon quality of life *Ann. Clin. Transl. Neurol.* **2** 864–72
[5] Espinosa D D and León-Ariza H 2025 Swimming performance with fins, hand paddles, and parachutes: a systematic review and meta-analysis *Sci. Sports* **41** 1–19
[6] Cortesi M, Di Michele R and Gatta G 2019 Effects of intracyclic velocity variations on the drag exerted by different swimming parachutes *J. Strength Cond. Res.* **33** 531–7
[7] White F M 2009 *Fluid Mechanics* (McGraw-Hill)
[8] Vogel S 1984 Drag and flexibility in sessile organisms *Integr. Comp. Biol.* **24** 37–44
[9] Coloretti V, Fantozzi S, Gatta G, Bonifazi M, Zamparo P and Cortesi M 2025 Quantifying added drag in swimming with parachutes: implications for resisted swimming training *J. Strength Cond. Res.* **39** e701–5
[10] Colado J C, Tella V and Triplett N T 2008 A method for monitoring intensity during aquatic resistance exercises *J. Strength Cond. Res.* **22** 2045–9
[11] Colado J C, Garcia-masso X, Rogers M, Tella V, Benavent J and Dantas E 2012 Effects of aquatic and dry land resistance training devices on body composition and physical capacity in postmenopausal women *J. Hum. Kinet.* **32** 185–95
[12] Colado C J, Borreani S, Pinto S S, Tella V, Martin F, Flandez J and Kruel L F 2013 Neuromuscular responses during aquatic resistance exercise with different devices and depths *J. Strength Cond. Res.* **27** 3384–90
[13] Haff G G 2010 Quantifying workloads in resistance training: a brief review *Prof. Strength Cond.* **19** 4–13
[14] Soligard T *et al* 2016 How much is too much? (Part 1) international Olympic committee consensus statement on load in sport and risk of injury *Br. J. Sports Med.* **50** 1030–41
[15] Impellizzeri F M, Menaspà P, Coutts A J, Kalkhoven J and Menaspà M J 2020 Training load and its role in injury prevention, Part I: back to the future *J. Athl. Train.* **55** 885–92
[16] Teasell R, Bitensky J, Salter K and Bayona N A 2005 The role of timing and intensity of rehabilitation therapies *Top. Stroke Rehabil.* **12** 46–57
[17] Sun J, Ke Z, Yip S P, Hu X L, Zheng X X and Tong K Y 2014 Gradually increased training intensity benefits rehabilitation outcome after stroke by BDNF upregulation and stress suppression *Biomed. Res. Int.* **2014** 925762
[18] Gosselin F, De Langre E and MacHado-Almeida B A 2010 Drag reduction of flexible plates by reconfiguration *J. Fluid Mech.* **650** 319–41
[19] Harder D L, Speck O, Hurd C L and Speck T 2004 Reconfiguration as a prerequisite for survival in highly unstable flow-dominated habitats *J. Plant Growth Regul.* **23** 98–107
[20] de Langre E, Gutierrez A and Cossé J 2012 On the scaling of drag reduction by reconfiguration in plants *C. R. Mec.* **340** 35–40
[21] Wu L, Wang H, Song Y, Zhang B, Xu Y, Liu C and Yan Y 2020 Drag reduction mechanism of *Paramisgurnus dabryanus loach* with self-lubricating and flexible micromorphology *Sci. Rep.* **10** 12873
[22] Ko H, Yu T-Y and Hu D L 2022 Fire ant rafts elongate under fluid flows *Bioinspir. Biomim.* **17** 045007
[23] Vogel S 1983 *The Physical Biology of Flow—Revised and Expanded Second Edition* (Princeton University Press) (https://doi.org/10.1515/9780691212975)
[24] Bekkers C C A, Angelou N and Dellwik E 2022 Drag coefficient and frontal area of a solitary mature tree *J. Wind Eng. Ind. Aerodyn.* **220** 104854
[25] Rahimi A M, Lustig S R, Bardhan J P and Jamali S 2022 Drag reduction and the Vogel exponent of a flexible beam in transient shear flows *Phys. Fluids* **34** 104111
[26] García-baena C, Camacho-sánchez J M, Lorite-díez M, Gutiérrez-montes C and Jiménez-gonzález

J I 2023 Drag reduction on a blunt body by self-adaption of rear flexibly hinged flaps *J. Fluids Struct.* **118** 103854
[27] Yang X, Liu M and Peng S 2014 Smoothed particle hydrodynamics and element bending group modeling of flexible fibers interacting with viscous fluids *Phys. Rev. E* **90** 063011
[28] Leclercq T and de Langre E 2016 Drag reduction by elastic reconfiguration of non-uniform beams in non-uniform flows *J. Fluids Struct.* **60** 114–29
[29] Luhar M and Nepf H M 2011 Flow-induced reconfiguration of buoyant and flexible aquatic vegetation *Limnol. Oceanogr.* **56** 2003–17
[30] York C A, Bartol I K, Krueger P S and Thompson J T 2020 Squids use multiple escape jet patterns throughout ontogeny *Biol. Open* **9** bio054585
[31] Silva A J, Rouboa A, Moreira A, Reis V M, Alves F, Vilas-Boas J P and Marinho D A 2008 Analysis of drafting effects in swimming using computational fluid dynamics *J. Sports Sci. Med.* **7** 60–66
[32] Jeon Y J, Yun J-H and Kang M-S 2022 Analysis of elastic properties of Al/PET isotropic composite materials using finite element method *Materials* **15** 8007
[33] Jin Y, Kim J-T, Cheng S, Barry O and Chamorro L P 2020 On the distinct drag, reconfiguration and wake of perforated structures *J. Fluid Mech.* **890** A1
[34] Whittaker P, Wilson C, Aberle J, Rauch H P and Xavier P 2013 A drag force model to incorporate the reconfiguration of full-scale riparian trees under hydrodynamic loading *J. Hydraul. Res.* **51** 569–80
[35] Kier W M 2016 The musculature of coleoid cephalopod arms and tentacles *Front. Cell Dev. Biol.* **4** 10
[36] Hou T G, Yang X B, Wang T M, Liang J H, Li S W and Fan Y B 2020 Locomotor transition : how squid jet from water to air Locomotor transition : how squid jet from water to air *Bioinspir. Biomim.* **15** 036014
[37] van Leeuwen J L and Kier W M 2023 Predicting the effects of spatiotemporal modifications of muscle activation on the tentacle extension in squid *Front. Bioeng. Biotechnol.* **11** 1193409
[38] Shimadzu H, Shibata R and Ohgi Y 2008 Modelling swimmers' speeds over the course of a race *J. Biomech.* **41** 549–55
[39] Fernandes A, Afonso J, Noronha F, Mezêncio B, Vilas-Boas J P and Fernandes R J 2023 Intracycle velocity variation in swimming: a systematic scoping review *Bioengineering* **10** 308
[40] Gourgoulis V, Antoniou P, Nikolaos A, Mavridis G, Kasimatis P, Vezos N, Boli A and Mavromatis G 2010 Kinematic characteristics of the stroke and orientation of the hand during front crawl resisted swimming *J. Sports Sci.* **28** 1165–73
[41] Zhang C, Zhou H, Xu L, Ru Y, Ju H and Chen Q 2022 Wind tunnel study of the changes in drag and morphology of three fruit tree species during air-assisted spraying *Biosyst. Eng.* **218** 153–62